FACILE SYNTHESIS AND ELECTRICAL CHARACTERISTICS OF n-SnO$_2$/p-NiO NANOWIRE HETEROJUNCTIONS

DANG THI THANH LE AND CHU MANH HUNG [†]

International Training Institute for Materials Science (ITIMS), Hanoi University of Science and Technology, No. 1 Dai Co Viet, Hanoi, Vietnam

[†]*E-mail:* mhchu@itims.edu.vn/hung.chumanh@hust.edu.vn

Abstract. *In the current work, we report a facile synthesis of n-SnO$_2$/p-NiO nanowire heterojunctions by a drop-coating approach. The pure SnO$_2$ and NiO nanowires (NWs) were grown by chemical vapor deposition (CVD) and hydrothermal methods, respectively. Morphology, composition and crystal structures of the NWs and heterojunctions were investigated by means of field emission scanning electron microscopy (FESEM), energy dispersive spectroscopy (EDS) and X-ray diffraction (XRD), respectively. The data showed that SnO$_2$ NWs were grown with their average diameter of 200 nm and length of about 15 µm. The NiO NWs were also synthesized with a shorter average length and smaller average diameter compared to those of the SnO$_2$ NWs. The EDS results indicated no impurity present in both SnO$_2$ and NiO NWs. The XRD patterns pointed out the tetragonal rutile and cubic structures of SnO$_2$ and NiO, respectively. Interestingly, electrical properties of the NWs and heterojunctions were studied through the Keithley 2602A sourcemeter-based $I - V$ characterizations. The results confirm the nature of the metal semiconducting oxides. The formation of the n-SnO$_2$/p-NiO heterojunctions was certified through the rectifying behavior of the I-V curves with the rectification ratio of about 5 at $\pm$ 3V and 350˚C. The potential energy barrier between the NWs was also estimated to be about 1.16 eV. The band energy structure was also proposed to get insight into characteristics of the n-SnO$_2$/p-NiO heterojunction.*

Keywords: SnO$_2$, NiO, p-n heterojunction, I-V characterization.

Classification numbers: 73.40.-c.

I. INTRODUCTION

In addition to a wide band energy (3.6 eV) and large exciton binding energy (130 meV), n-type SnO$_2$ semiconducting nanostructures with the simultaneous appearance of transparency and conductivity feature, have been widely used as transparent conductors in solar cell, light emitting diodes, photocatalytic, and gas sensors [1, 2]. Along with such n-type material, much attention has been also paid for p-type NiO nanostructures owing to their interesting properties such as a wide band gap of 3.8 eV, smaller electron affinity, low resistivity, and stable p-type semiconductor characteristics [3, 4]. Therefore, it has been widely applied in resistive switching memory device, electrode for lithium ion battery application as well as a transparent p-type conducting layer for hole carriers [3, 5]. However, the efficiency of the pure n- and p-type oxide-based devices are still low [6]. As a promising way to improve the performance of the devices, in recent years, fabrication of heterojunction structures between p- and n-type semiconductor oxides have been investigated extensively [7–9]. For example, Zhang *et al.* improved photocatalytic efficiency of semiconductor oxide nano-catalysts by forming p-NiO/n-ZnO heterojunction structures. Mutual transfer of photogenerated electrons or holes at the heterojunctions allowed to hinder the recombination of photogenerated electron-hole pairs and therefore improve the photocatalytic efficiency [7]. While Ohta *et al.* reported a good photo-response of diodes based on $p-n$ heterojunction semiconductor oxides, that makes the heterojunction diode is suitable for portable UV detector application [8]. Regarding the sensor application, the nanojunction structures were used to enhance the gas-sensing efficiency through the variation in barrier height between p- and n-type material contacts [10]. However, these $p-n$ heterojunction structures were grown using sophisticated equipments such as pulsed-laser deposition combined with a solid-phase-epitaxy [8] and electro-spinner [7]. Apart from the studies on the p-NiO/n-ZnO heterojunctions, from the literature review, some reports also presented the $p-n$ heterojunction structures of NiO with SnO$_2$ [11, 12], but existing as composite nanofibers. It means that the heterojunctions were generated within each nanofiber. In addition, these studies focused mainly on the gas sensing properties of the synthesized materials but not on the electrical properties of the p-NiO/n-SnO$_2$ heterojunctions.

Therefore, in this research we present a simple and low-cost method (hydrothermal and chemical vapor deposition methods in combination with a drop-coating process) for preparation of heterojunction structures between the n-type SnO$_2$ NWs and p-type NiO NWs for their electrical property investigation. The pure SnO$_2$, NiO NWs were synthesized by a chemical vapor deposition (CVD) and hydrothermal methods, respectively. The morphological, compositional, structural, and detailed electrical properties of the pure SnO$_2$, NiO NWs and the SnO$_2$/NiO heterojunctions were studied. Through the measured electrical properties, the $p-n$ heterojunctions showed good $I-V$ rectifying characteristics and the potential barrier height of about 1.16 eV.

II. EXPERIMENT

n-SnO$_2$/p-NiO nanowire heterojunctions were simply fabricated through three steps. First, SnO$_2$ NWs were grown on Pt electrodes by CVD method as illustrated in Fig. 1(a). A ceramic boat containing 0.2g Sn powder (purity of 99.8%) and Pt electrodes were placed at the center and 10 cm from center of a quartz tube in the horizontal furnace, respectively. Before heating, the tube was sucked as well as purged with Ar gas at a flow rate of 300 sccm for 10 min. The furnace was then heated to 750˚C with the rate of 36˚C/min. As soon as reached the temperature of 750˚C, the

oxygen gas was introduced in the tube with a rate of 0.5 sccm at the pressure of 1.6×10^{-1} Torr for growth of SnO$_2$ NWs for 10 min. A detailed deposition process can be found elsewhere [13]. Secondly, Ni(OH)$_2$ NWs were synthesized via a typical procedure as shown in Fig. 1(b). 0.474 g NiCl$_2$.6H$_2$O (Sigma-Aldrich) and 0.12 g Na$_2$C$_2$O$_4$ (Sigma-Aldrich) were dissolved in a mixed solution of 32 ml ethylene glycol and 18 ml DI water to obtain a clear light-green solution. The solution was then transferred to a 100 ml-volume Teflon autoclave and the hydrothermal process took place at 200˚C for 24 h. After the growth, the precipitated Ni(OH)$_2$ NWs were collected and washed with DI water and ethanol to remove contaminated and unexpected ions. NiO NWs can be then formed by a calcination process of the Ni(OH)$_2$ precipitation at 500˚C for 2 h. Finally, Fig.1(c) illustrates a simple process to fabricate the n-SnO$_2$/p-NiO nanowire heterojunctions. The washed 0.01 g Ni(OH)$_2$ precipitation was dispersed in the 2 g dimethylformamide (DMF) solution through a ultrasonic bath. This solution was dropped on the surface of the grown SnO$_2$ NWs. The Pt electrodes with the SnO$_2$/ Ni(OH)$_2$ NWs on their surface were dried at 150˚C for 30 min before calcinating at 500˚C to produce SnO$_2$/NiO heterojunctions.
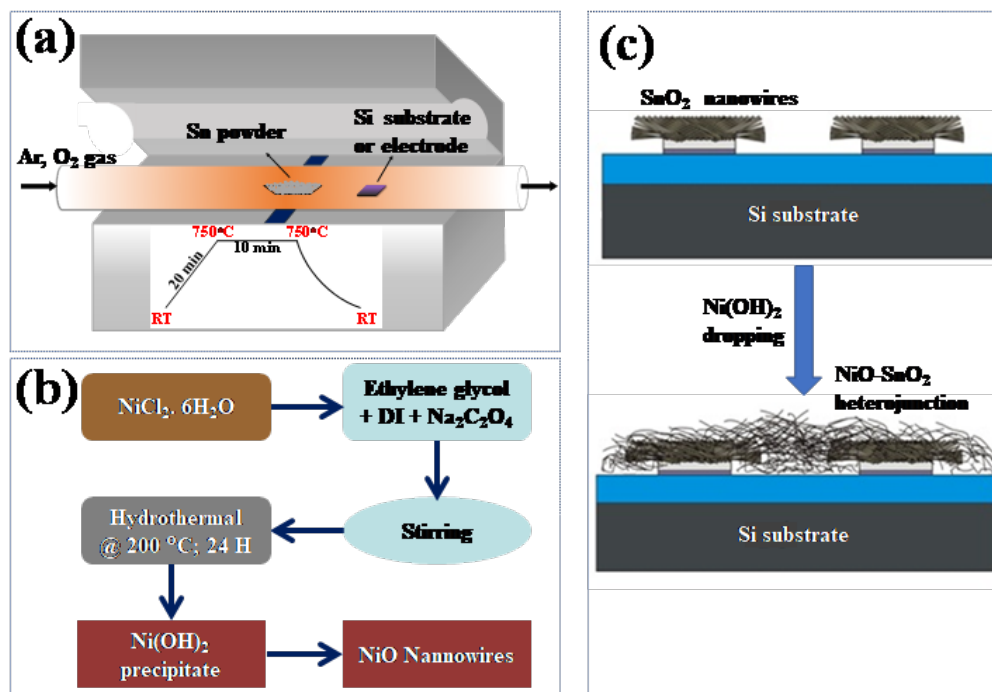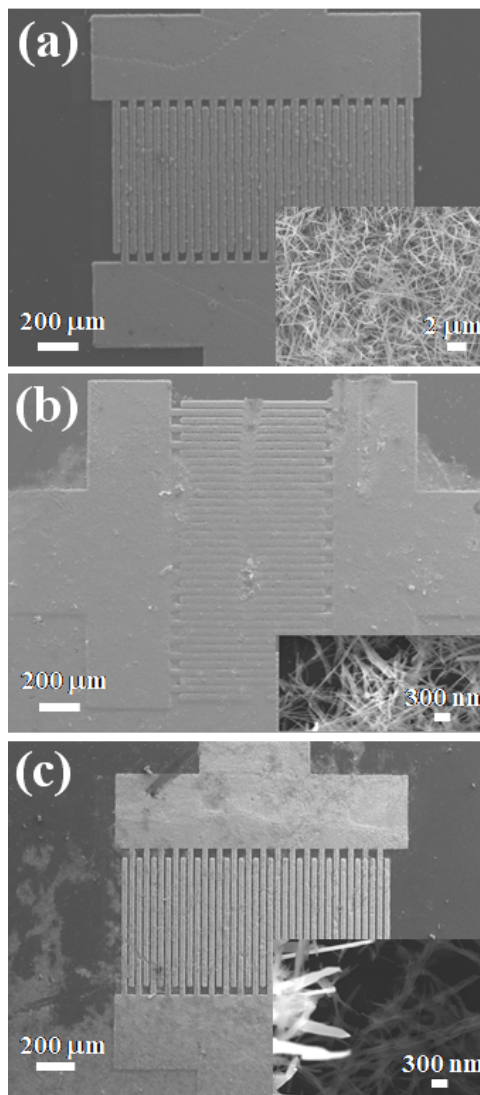

Fig. 1. Schematic illustrations of (a) CVD system for deposition of SnO$_2$ NWs, (b) hydrothermal processes for the synthesis of NiO NWs, and (c) a drop-coating process for formation of n-SnO$_2$/p-NiO nanowire heterojunctions.

The morphological, compositional and crystal structure properties of the SnO$_2$, NiO NWs, and NiO/SnO$_2$ heterojunctions were investigated by the FESEM (JEOL JSM-7600F), EDS, and XRD (Cu-K$_\alpha$ radiation = 0.154 nm), respectively. Electrical properties of the NWs and heterojunctions were characterized by a Keithley 2602A model sourcemeter.

III. RESULTS AND DISCUSSION

Fig. 2 shows the FESEM images of the Pt electrodes deposited with the SnO$_2$, NiO NWs, and *n*-SnO$_2$/*p*-NiO heterojunctions grown by the CVD, hydrothermal, and drop-coating methods, respectively. Fig. 2(a) reveals that the SnO$_2$ NWs were synthesized on all the surface of the Pt electrodes. The inset of Fig. 2(a) is a higher magnification FESEM image, which indicates the average length and diameter of SnO$_2$ NWs are about 15 μm and 200 nm. Similarly, Fig. 2(b) displays low- and high-magnification FESEM images of NiO NW-based Pt electrodes and NiO NWs. The length and diameter of NiO NWs are shorter and smaller than those of SnO$_2$ NWs. By dropping the Ni(OH)$_2$ solution on the surface of SnO$_2$ NW-based Pt electrodes and followed by the calcination process, the *n*-SnO$_2$/*p*-NiO NW heterojunctions were produced as shown in Fig. 2(c).

To confirm the elemental composition of the synthesized structures, the EDS measurements were carried out. Fig. 3(a) reveals the EDS spectra of the SnO$_2$ (upper part) and NiO NWs (lower part). The upper EDS spectrum indicates the presence of Si from the substrate and the Sn, O elements from the SnO$_2$ NWs. Similarly, the EDS spectrum in the lower panel displays the existence of Ni and O elements in the NiO NWs without any contaminations. The crystal structure of the NWs was studied through the XRD measurement. Fig. 3(b) presents the XRD spectra of the SnO$_2$ and NiO NWs. The XRD pattern (on top) is indexed to the tetragonal rutile structure of SnO$_2$, which is in agreement with the reported data (JCPDS File No. 77-0450) [14]. While the XRD data (at the bottom) shows that the NWs were crystallized in the *Fm3m* space group for NiO structure (JCPDS no. 47 − 1049) [15].

Fig. 2. Low and high magnification FESEM images of (a) SnO$_2$, (b) NiO NWs, and (c) n-SnO$_2$/p-NiO heterojunctions grown on Pt electrodes.

Both XRD patterns reveal sharp peaks for a single phase for SnO$_2$ and NiO NWs without any impurity and secondary phases. It confirms that the NWs grown by CVD and hydrothermal methods were well-crystalline pure SnO$_2$ and NiO with

the small crystallite size, respectively. Namely, the average grain size of the SnO_2 and NiO NWs was estimated by the Scherrer formula:

$$D = \frac{0.9\lambda}{\beta \cos \theta},$$

where D is the mean grain size, λ is the wavelength of X-ray radiation = 0.154 nm, β and θ are the full width at half maximum and Bragg angle of a diffracted peak, respectively. According to the highest XRD peaks for (101) and (200) planes of the SnO_2 and NiO NWs, respectively, the calculated average grain size is 15.07 nm for SnO_2 NWs and 10.64 nm for NiO NWs. As discussed above, the SnO_2 and NiO NWs, with average diameters of a few hundred nanometers, may exist grain boundaries, which can affect their electrical properties.
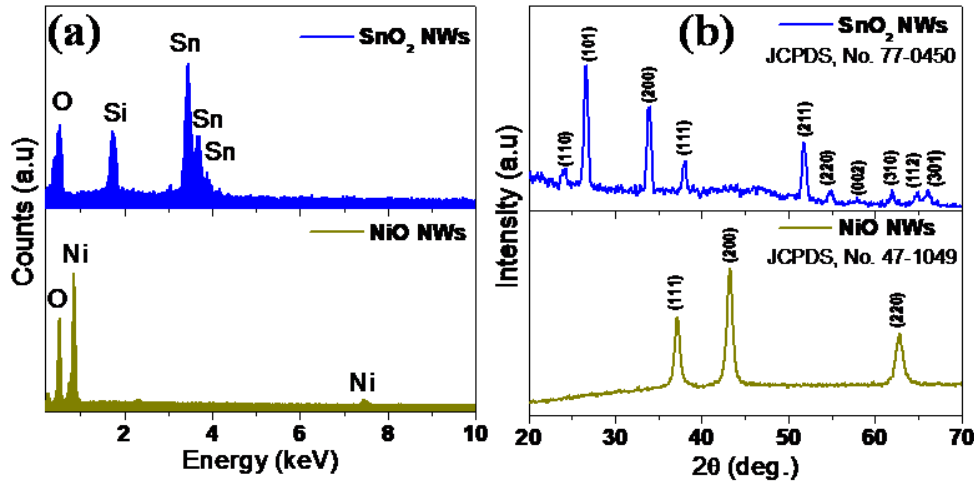
Fig. 3. (a) EDS spectra of the SnO_2 (upper panel) and NiO NWs (lower panel); (b) XRD patterns of the SnO_2 (upper) and NiO NWs (lower).

The electrical properties of the as-grown NWs and SnO_2/NiO heterojunctions were characterized at various temperatures ranging from 150 to 350°C and different applied bias voltages from -3 to 3 V using the Keithley 2602A sourcemeter. The typical $I - V$ characteristics of the pure SnO_2, NiO NWs, and SnO_2/NiO heterojunctions are shown in Figs. 4(a), 4(b) and 4(c), respectively. As can be seen in Fig. 4(a), the $I - V$ curves of the pure SnO_2 NWs reveal a quasi-linear behavior, implying the existence of a small Schottky barrier between the NWs and Pt electrodes. It may be due to a reason that the Pt electrodes were put in the furnace during the on-chip growth of the SnO_2 NWs at the high temperature, which can influence on the contact between the NWs and the electrodes and/or the quality of Pt film electrodes. On the other hand, Fig. 4(b) indicates a perfect linear behavior of the $I - V$ characteristics of the NiO NWs, confirming a good ohmic contact between the NWs and Pt electrodes. It is worth to recall that the NW-electrode contact in this case was formed at the room temperature first through the drop-coating method and followed by a calcination process at a much lower temperature than the on-chip growth temperature of the SnO_2 NWs, leading to a good contact between the NWs and electrodes. Both Fig. 4(a) and Fig. 4(b)

indicate that the conductivity of the NWs increases with the increase of the temperature, reflecting a nature of metal semiconducting oxides.

The $I - V$ characteristic of the n-SnO$_2$/p-NiO heterojunctions is shown in Fig. 4(c). Similarly, when the temperature increased from 150 to 350˚C, the current in the heterojunctions also increases. More interestingly, the $I - V$ curves shows a rectifying behavior with a rectification ratio (calculated as forward current/reverse current ratio) of ~ 5 at ± 3 V and 350˚C. With increasing temperature, the rectifying effect becomes clearer and dominant. The non-linear $I - V$ characteristics indicate that the $p - n$ junction between SnO$_2$ and NiO NWs was formed and therefore a potential-barrier was formed a potential-energy barrier. This barrier height can be calculated using the following equations [16, 17]:
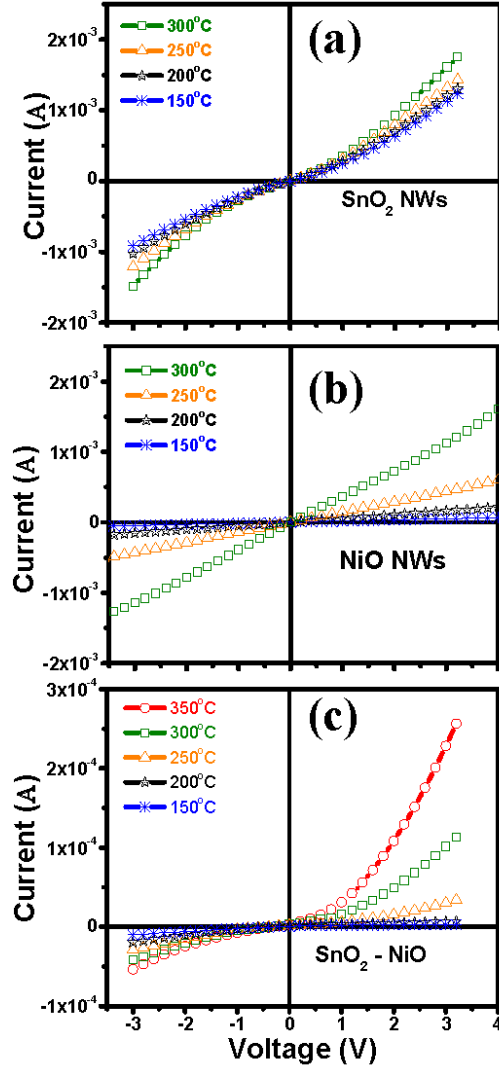
$$\Phi_B = \frac{kT}{q} \ln \left(\frac{AA^\star T^2}{I_0} \right),$$

where φ_B is the barrier height, k is the Boltzmann constant, T is the absolute temperature, q is the electron charge, I_0 is the saturation current, A^* is the Richardson constant, and A is the device area. The Richardson constant

$$A^\star = \frac{4\pi em^\star \kappa_B^2}{h^3} = 120 \frac{m^\star}{m_0} A \ \text{cm}^{-2}\text{K}^{-2},$$
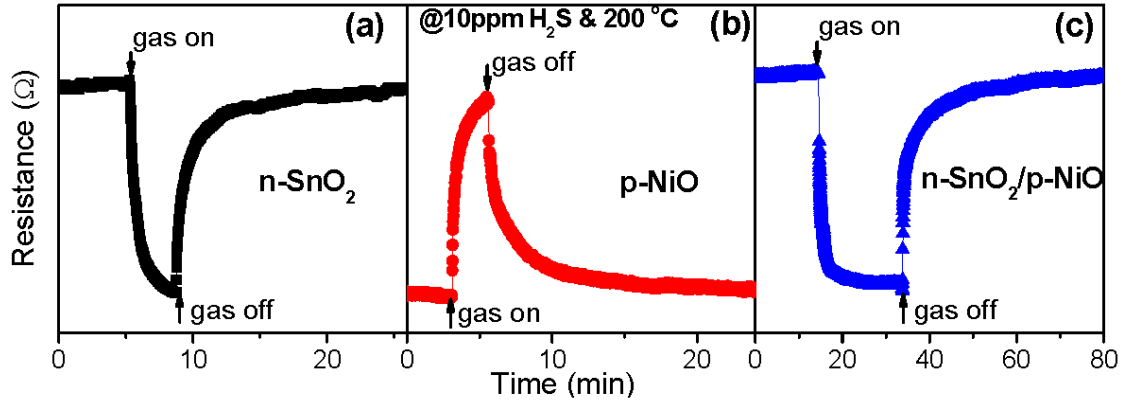
where $m^\star$ is the effective mass and m_0 is the rest mass with $m^\star = 0.55 m_0$ [18–20]. Therefore, the estimated barrier height is approximately 1.16 eV. This calculation is valuable for future research related to diode/laser/sensor applications.

In order to confirm the main carrier type of the n-SnO2/p-NiO heterojunction, Fig.5 shows the comparison in resistance response type of the n-SnO$_2$, p-NiO, and n-SnO2/p-NiO heterojunction sensors toward the 10 ppm H$_2$S at 200˚C. The data present the changes in resistance when flowing and stop flowing H$_2$S gas

Fig. 4. I-V characteristics of the (a) SnO$_2$, (b) NiO NWs, and (c) SnO$_2$/NiO heterojunctions at various temperatures.

to surface of these materials, which was based on the surface oxygen adsorption mechanism [13]. When the semiconductor materials put in air and at the 200˚C, there will be O$_2^-$ and O$^-$ existing on the surface of the semiconductor [21]. In the case of pure SnO$_2$ NW based sensor (Fig. 5(a)),

the main carrier is electron (e^-) owing to its n-type semiconducting property. Once the H$_2$S is introduced to the sensor, it adsorbed with oxygen species by two following reactions:

$$2H_2S_{(gas)} + 6O^-_{(ads)} = 2H_2O_{(gas)} + 2SO_{2(gas)} + 6e^- \tag{1}$$

$$2H_2S_{(gas)} + 3O^-_{2(ads)} = 2H_2O_{(gas)} + 2SO_{2(gas)} + 3e^- \tag{2}$$

Fig. 5. Transient resistance response of gas sensors based on (a) *n*-SnO$_2$, (b) *p*-NiO, and (c) *n*-SnO$_2$/*p*-NiO heterojunction upon exposure to 10 ppm H2S at 200˚C.

As we can see that after reaction, additional electrons are provided, which contribute to increase the main carrier in the *n*-SnO$_2$. Therefore, the resistance of the sensor was decreased. Conversely, Fig. 5(b) shows that the resistance response of the pure NiO NW based sensor increased by introducing the H$_2$S gas to the surface of the materials. It can be explained similarly to the case of *n*-SnO$_2$ NWs, however in the case of *p*-NiO NWs, hole plays a role as its main carrier. When the H$_2$S gas absorbed to the surface of the NiO NWs, more electrons are generated. Thus, resistance of the sensor was increased upon exposure to the H$_2$S gas in case of *p*-NiO NW. Fig. 5(c) reveals the transient resistance response of the *n*-SnO$_2$/*p*-NiO heterojunction sensor, which indicates an identical trend to the one of the *n*-SnO$_2$ sensor when the H$_2$S gas was introduced to the surface of the sensor. It suggests that main carrier type of the SnO$_2$/NiO heterojunction is electron, which is in agreement with previous report [11].

To get further insight into the *n*-SnO$_2$/*p*-NiO heterojunctions, Fig. 6 schematically illustrates the energy band structure of the SnO$_2$-NiO junction. Band gap energies of SnO$_2$ and NiO nanostructures are taken from works using similar CVD and hydrothermal growth methods, respectively [4, 22]. It is well known that at equilibrium there is only one Fermi level in the heterojunction structure. However, the Fermi level of the *n*-type SnO$_2$ and *p*-type NiO locates at different positions. In addition, these two metal oxides have different band gap energy as shown in Fig. 6. Therefore, to equalize the Fermi level, the relative motion of carriers, including the movement of electrons from SnO$_2$ to NiO and holes from NiO to SnO$_2$, results in a band bending and a depletion layer [23]. This will generate a potential energy barrier calculated to be approximately 1.16 eV between the two metal oxides.
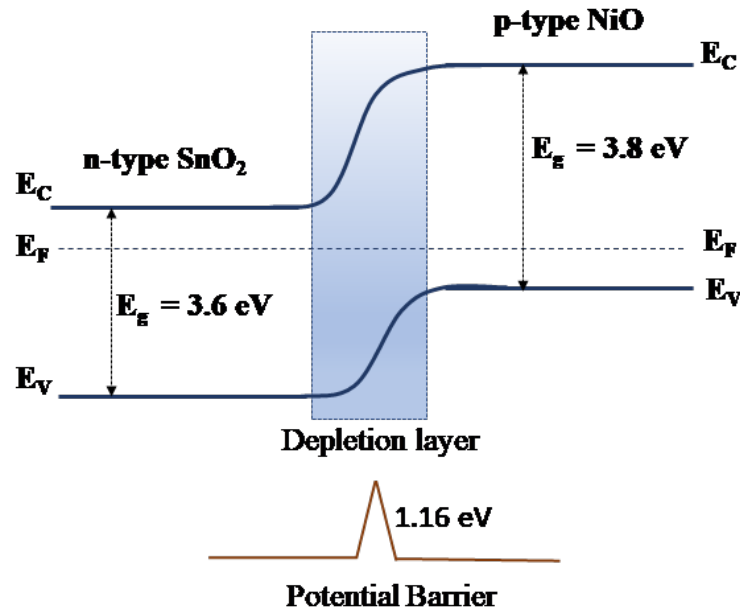
Fig. 6. Proposed energy band structure of the n-SnO$_2$/p-NiO heterojunctions.

IV. CONCLUSION

The *n*-SnO$_2$/*p*-NiO nanowire heterojunction structures were successfully synthesized through a drop-coating approach. The pure SnO$_2$ and NiO NWs with the tetragonal rutile and cubic structures were grown by CVD and hydrothermal methods, respectively. The average grain sizes of the SnO$_2$ and NiO NWs were about 15.07 nm and 10.64 nm. By means of the Keithley 2602A sourcemeter, the electrical properties of the SnO$_2$, NiO NWs, and the SnO$_2$/NiO heterojunctions were studied. The findings in the pure NWs showed a good ohmic contact between NiO NWs and Pt electrodes, while there is the existence of a small Schottky barrier between the SnO$_2$ NWs and the electrodes. The $I - V$ characterization of the *n*-SnO$_2$/*p*-NiO junctions evidences their rectifying properties with the rectification ratio of ∼5 at ± 3 V and 350˚C. Potential energy barrier between the *n*-type and *p*-type NWs was estimated to be about 1.16 eV. The synthesized heterojunction structures are expected to play a crucial role for improving the performance of future diode/gas sensor devices.

REFERENCES

[1] R. Chen, G. Z. Xing, J. Gao, Z. Zhang, T. Wu, H. D. Sun, *Appl. Phys. Lett.* **95** (2009) 69.
[2] S. Das, V. Jayaraman, *Prog. Mater. Sci.* **66** (2014) 112.

[3] B. O. Jung, Y.H. Kwon, D. J. Seo, D. S. Lee, H. K. Cho, *J. Cryst. Growth.* **370** (2013) 314.

[4] L. Kumari, W. Z. Li, C. H. Vannoy, R. M. Leblanc, D. Z. Wang, *Journal of Experimental and Industrial Crystallography* **44** (2009) 495.

[5] D. C. Kim, S. Seo, S.E. Ahn, D. S. Suh, M. J. Lee, B. H. Park, I. K. Yoo, I. G. Baek, H. J. Kim, E. K. Yim, J. E. Lee, S. O. Park, H. S. Kim, U. I. Chung, J. T. Moon, B. I. Ryu, *Appl. Phys. Lett.* **88** (2006) 202102.

[6] Y. Shen, X. Yan, H. Si, P. Lin, Y. Liu, Y. Sun and Y. Zhang, *ACS Appl. Mater. Interfaces* **8** (2016) 6137.

[7] Z. Zhang, C. Shao, X. Li, C. Wang, M. Zhang, Y. Liu, *ACS Appl. Mater. Interfaces* **2** (2010) 2915.

[8] H. Ohta, M. Hirano, K. Nakahara, H. Maruta, T. Tanabe, M. Kamiya, T. Kamiya and H. Hosono, Appl. Phys. Lett. **83** (2003) 1029.

[9] C. Liu, M. Peng, A. Yu, J. Liu, M. Song, Y. Zhang and J. Zhai, *Nano Energy* **26** (2016) 417.

[10] Q. T. Minh Nguyet, N. Van Duy, N. T. Phuong, N. N. Trung, C. M. Hung, N. D. Hoa and N. V. Hieu, *Sensors Actuators, B Chem.* **238** (2017) 1120.

[11] Z. Wang, Z. Li, J. Sun, H. Zhang, W. Wang, W. Zheng and C. Wang, *J. Phys. Chem. C* **114** (2010) 6100.

[12] Y. Wang, H. Zhang and X. Sun, *Appl. Surf. Sci.* **389** (2016) 514.

[13] C. M. Hung, D. T. T. Le and N. V. Hieu, *J. Sci. Adv. Mater. Devices* **2** (2017) 263.

[14] D. D. Trung, N. Van Toan, P. Van Tong, N. Van Duy and N. Duc, *Ceram. Int.* **38** (2012) 6557.

[15] M. Ghosh, K. Biswas, A. Sundaresan and C. N. R. Rao, *J. Mater. Chem.* **16** (2006) 106.

[16] R. Singh and A. K. Narula, *Appl. Phys. Lett.* **71** (1997) 2845.

[17] R.K.Ã. Gupta, K. Ghosh and P. K. Kahol, **41** (2009) 617.

[18] S. K. Sharma, B. Bhowmik, V. Pal and C. Periasamy, *IEEE Sensors J.* **17** (2017) 7332.

[19] C. A. Amorim, E. P. Bernardo, E. R. Leite and A. J. Chiquito, *Semicond. Sci. Technol.* **33** (2018) 055003.

[20] C. Rödl and A. Schleife, *Phys. Status Solidi.* **211** (2014) 74.

[21] P. Rai and Y. Yu, *Sensors Actuators B. Chem.* **173** (2012) 58.

[22] W. Yin, B. Wei and C. Hu, *Chem. Phys. Lett.* **471** (2009) 11.

[23] W. Tang and J. Wang, *Electron. Mater. Lett.* **2016** (2016) 172.